CrossMark

The Met80Ala and Tyr67His/Met80Ala mutants of human cytochrome c shed light on the reciprocal role of Met80 and Tyr67 in regulating ligand access into the heme pocket

Chiara Ciaccio [a,c,1], Lorenzo Tognaccini [b,1], Theo Battista [a], Manuela Cervelli [d], Barry D. Howes [b], Roberto Santucci [a], Massimo Coletta [a,c], Paolo Mariottini [d], Giulietta Smulevich [b,c,*], Laura Fiorucci [a,*]

[a] Department of Clinical Sciences and Translational Medicine, University of Rome Tor Vergata, Rome, Italy
[b] Department of Chemistry "Ugo Schiff", University of Florence, Sesto Fiorentino, FI, Italy
[c] Interuniversity Consortium for the Research on the Chemistry of Metals in Biological Systems (CIRCMSB), Bari, Italy
[d] Department of Sciences, University of Rome Tre, Rome, Italy

ARTICLE INFO

ABSTRACT

The spectroscopic and functional properties of the single Met80Ala and double Tyr67His/Met80Ala mutants of human cytochrome c have been investigated in their ferric and ferrous forms, and in the presence of different ligands, in order to clarify the reciprocal effect of these two residues in regulating the access of exogenous molecules into the heme pocket. In the ferric state, both mutants display an aquo high spin and a low spin species. The latter corresponds to an OH^- ligand in Met80Ala but to a His in the double mutant. The existence of these two species is also reflected in the functional behavior of the mutants. The observation that (i) a significant peroxidase activity is present in the Met80Ala mutants, (ii) the substitution of the Tyr67 by His leads to only a slight increase of the peroxidase activity in the Tyr67His/Met80Ala double mutant with respect to wild type, while the Tyr67His mutant behaves as wild type, as previously reported, suggests that the peroxidase activity of cytochrome c is linked to an overall conformational change of the heme pocket and not only to the disappearance of the Fe-Met80 bond. Therefore, in human cytochrome c there is an interplay between the two residues at positions 67 and 80 that affects the conformation of the distal side of the heme pocket, and thus the sixth coordination of the heme.

© 2017 Elsevier Inc. All rights reserved.

1. Introduction

Cytochrome c (cyt c) is a single-chain hemoprotein (12.5 kDa) lying in the inter-membrane space of the eukaryotic mitochondria, where it plays a role as an electron carrier and as a ROS scavenger [1,2]. It is composed of 104 amino acids and contains a heme c prosthetic group. The heme lies within a crevice and is covalently attached to the polypeptide chain by two thioether bridges formed with the Cys14 and Cys17 residues. His18 and Met80 are the fifth and sixth axial ligands, respectively, of the heme iron in the native protein.

Recent studies on cyt c have highlighted the multiple functions carried out by this protein in cells. Such functions seem to be strictly regulated by distinct mechanisms: expression of different isoforms, reversible phosphorylation and, remarkably, protein conformational changes in response to different cell stimuli. In particular, direct interaction with cardiolipin (CL), a phospholipid of the mitochondrial membrane, gives rise to a more flexible tertiary structure, disruption of the Met80-heme iron ligation, gain of peroxidase activity and release into the cytosol [3,4]. Transition to alternative conformations and acquisition of peroxidase activity are thought to further enable the multiple functions of cyt c and its translocation across cellular compartments (cytosol and even nucleus) [5,6]. The release of cyt c from mitochondria into the cytosol upon CL peroxidation is an important apoptotic trigger [7,8]. The identification of these alternative conformations and characterization of the structural features that determine the flexibility of the cyt c-CL complex, which confer to the protein important roles in "life" and "death" processes, continue to be a major challenge [9,10].

The Met80 residue is located in the surface heme crevice loop (residues 71–85), the most highly conserved segment of the primary structure of cyt c. The dynamics of the heme crevice loop are regulated by its link with the 40–57 loop through Tyr67. In fact, Tyr67, a highly conserved residue, forms a hydrogen bond network with Met80 and other conserved residues (such as Asn52 and Thr78). This hydrogen bond network helps to maintain the sulfur atom of Met80 in the right position as the heme iron ligand, thus also controlling the redox potential of the protein. Moreover, mutations at the Tyr67 position have been previously shown to lead to a rearrangement of the distal portion of the heme cavity, depending on the type of substituting residue [11,12]. In human cyt c, substitution of Tyr67 by Arg leads to the cleavage of the Met80 heme bond and to an increased peroxidase activity, while substitution by His affects the heme pocket to a much lower extent and the Tyr67His mutant seems to have no significant peroxidase activity [13,14]. Strikingly, in yeast cyt c, the Tyr67His mutant has been reported to have significant peroxidase activity, possibly acting as a distal histidine and general acid-base catalyst in the distal heme pocket [15].

Indeed, recent findings on various cyt c proteins from higher eukaryotes reveal the presence of more sterically bulky amino acids in the heme crevice loop with respect to yeast cyt c. These features may be responsible for the slow opening of the heme crevice loop and reduced loss of Met80 ligation in human cyt c, suggesting that the heme crevice loop has evolved to minimize undesirable peroxidase activity [10,16,17].

To gain better insight into the role of Met80-Fe ligation in the structure and function of cyt c, we have generated two cyt c variants, namely the single Met80Ala (MA) and double Tyr67His/Met80Ala (YHMA) mutants, and investigated their spectroscopic and functional properties.

2. Materials and methods

2.1. Materials

Gaseous ^{12}CO and ^{13}CO were purchased from Rivoira and FluoroChem, respectively. Sodium dithionite was obtained from Fluka Biochemika. All the other chemicals were obtained from Aldrich, Steinheim, Germany. All chemicals were of analytical or reagent grade and were used without further purification.

2.2. Methods

2.2.1. Expression and site-directed mutagenesis of recombinant human cytochrome c

The plasmid pBTR(hCc) [18] was transformed into E. coli strain BL21(DE3).

To make mutants of the human cyt c protein, site-directed mutagenesis was carried out on the plasmid pBTR(hCc) using the QuikChange™ Site-directed Mutagenesis kit (Stratagene) and following the manufacturer's protocol. The introduction of mutations into the nucleotide sequences was confirmed by sequence analysis. The procedures are outlined briefly in the Supplementary information together with the primer sequences used in this work (Table S1). Purification of the recombinant proteins was conducted as previously described [13]. After purification the proteins were concentrated and stored in 0.1 M phosphate buffer at pH 7.0. The homogeneity of the wild type (WT) human cyt c and mutants (i.e., Met80Ala (MA) and Tyr67His-Met80Ala (YHMA)) were determined by running SDS-PAGE. Recombinant WT human cyt c was used as a control in all the experiments described and reported herein as WT.

2.2.2. Sample preparation

The samples at pH 7.0 were obtained by 1:1 dilution of the purified proteins with 0.1 M phosphate buffer at pH 7.0, at pH 6 by 3:1 dilution with 0.1 M phosphate buffer at pH 7.0 and 0.125 M citrate buffer at pH 4.3, and at pH 5.5 by 1.9:1 dilution with 0.1 M phosphate buffer at pH 7.0 and 0.125 M citrate buffer at pH 4.3.

To ensure complete oxidation, 1–3 μL of a 3 mM freshly prepared $K_4[Fe(CN)_6]$ solution were added to 40 μL protein samples.

The pure ferric form of the MA mutant was obtained by a reduction and re-oxidation process. The sample solution was reduced by adding dithionite powder, excess dithionite being removed by 2 h dialysis in fresh buffer; the sample was then oxidized by adding a few grains of $K_4[Fe(CN)_6]$, excess $K_4[Fe(CN)_6]$ being removed by dialyzing overnight.

The cyt c-imidazole (ImH) complex was prepared according to Oellerich et al. [19]. Briefly, 75 mM SDS (sodium dodecyl sulfate) solution was added to a horse heart cyt c (HH cyt c) solution in 50 mM phosphate buffer (pH 7.0) followed by addition of a 0.1 M imidazole solution (pH 7.0); the SDS concentration in the resulting mixture was 13–14 mM and the cyt c: imidazole molar ratio was 1:2500.

Ferrous samples were prepared by addition of 2–3 μL of a freshly prepared sodium dithionite (10 mg/mL) solution to the ferric forms (40 μL) previously degassed with nitrogen. It is noted that the double YHMA variant easily oxidized at pH lower than 7.

The CO complexes were prepared by degassing the ferric protein solution by flushing firstly with nitrogen, then with ^{12}CO or ^{13}CO and reducing the heme by addition of 2–3 μL of a freshly prepared sodium dithionite (10 mg/mL) solution.

Protein concentrations in the range 15–50 μM were used for the electronic absorption and RR samples. The protein concentration was determined on the basis of the molar absorptivity (ε) of 106 mM^{-1} cm^{-1} at 409 nm for the WT protein [20,21] and of 121.7 mM^{-1} cm^{-1} at 405 nm for the MA, and YHMA mutants [22].

For the CD experiments, the samples (7 μM heme in the Fe(III) form both for WT and mutants) were prepared in 0.1 M phosphate buffer pH 7.0.

2.2.3. Electronic absorption measurements

Electronic absorption spectra, measured with a Cary 60 (Agilent Technologies) at 25 °C, were recorded using a 1-cm cuvette and a 300 nm/min scan rate. Absorption spectra (using a 5-mm NMR tube) were measured both prior to and after RR measurements to ensure that no degradation had taken place under the experimental conditions used. For the differentiation process, the Savitzky–Golay method was applied using 15 data points (LabCalc, Galactic Industries, Salem, NH). No changes in the wavelength or in the bandwidth were observed when the number of points was increased or decreased.

2.2.4. Circular dichroism (CD) spectroscopy

CD spectra in the far-UV (200–250 nm) and Soret (400–450 nm) regions were recorded using a Jasco-710 spectropolarimeter (Tokyo, Japan) equipped with a PC as data processor and a temperature-controlled holder maintained at 25 °C. Quartz cells with 1- and 5-mm path lengths were used for measurements in the far-UV and Soret regions, respectively. The molar ellipticity (deg·cm^2·dmol^{-1}) is expressed as $[\Theta]_h$ on a molar heme basis in the Soret region and as mean residue ellipticity $[\Theta]_a$ in the far-UV region (mean residue relative molecular mass 119 g/mol). The spectra were acquired with 0.5 nm/min resolution and four scans per spectrum.

2.2.5. Resonance Raman (RR) spectroscopy

RR spectra were recorded using a 5-mm NMR tube and 406.7, 413.1 nm (Kr$^+$ laser, Innova300 C, Coherent, Santa Clara, CA) and 441.6 nm (He-Cd, Kimmon IK4121R-G) excitation wavelengths. Backscattered light from a slowly rotating NMR tube was collected and focused into a triple spectrometer (consisting of two Acton Research SpectraPro 2300i and a SpectraPro 2500i in the final stage with a grating of 3600 or 1800 grooves/mm) working in the subtractive mode, equipped with a liquid nitrogen-cooled CCD detector. A spectral resolution of 1.2 cm^{-1} and spectral dispersion of 0.4 cm^{-1}/pixel were calculated theoretically on the basis of the optical properties of the

spectrometer for the 3600 grating; for the 1800 grating, used to collect the RR spectra in the 2000–2300 cm^{-1} region of the CO complexes, the spectral resolution was 4 cm^{-1} and spectral dispersion 1.2 cm^{-1}/pixel.

The spectra of the CO complexes have been obtained using a cylindrical lens, which focuses the laser light into a line instead of a point, to minimize ligand photolysis.

The RR spectra were calibrated with indene, n-pentane and carbon tetrachloride as standards to an accuracy of 1 cm^{-1} for intense isolated bands. All RR measurements were repeated several times under the same conditions to ensure reproducibility. To improve the signal-to-noise ratio, a number of spectra were accumulated and summed only if no spectral differences were noted. The samples of the mutated proteins were cooled by a gentle flow of N$_2$ gas (sample temperature about 12 °C) during the RR measurement. All spectra were baseline-corrected. A curve-fitting program (LabCalc, Galactic) was used to simulate the spectra using a Lorentzian line shape in order to determine peak bandwidths and positions. The frequencies of the bands were optimized with an accuracy of 1 cm^{-1}, and the bandwidths with an accuracy of 0.5 cm^{-1}.

2.2.6. Peroxidase activity assay

The peroxidase activities of WT and mutants were determined by measuring the H$_2$O$_2$-dependent oxidation at different concentrations of the substrate guaiacol. The steady-state kinetics of guaiacol oxidation to give its tetramer was measured spectrophotometrically at 470 nm and 25 °C ($\varepsilon_{470\ nm} = 26.6$ mM^{-1} cm^{-1}) [23]. The reaction mixture contained the protein at a final concentration of 1 μM in 0.1 M phosphate buffer pH 7.0 and a guaiacol concentration ranging between 10 μM and 200 μM. The reaction was initiated by addition of H$_2$O$_2$ (0.1 mM or 1 mM) to the reaction mixture.

2.2.7. Kinetic measurements

Kinetic measurements have been carried out by rapid-mixing experiments using the SX18.MV stopped-flow apparatus (Applied Photophysics, Salisbury, UK) equipped with a diode array for spectra acquisition over a 1 ms time range. Ligand binding experiments have been undertaken by mixing the Fe(II) or Fe(III) forms (at a heme concentration of 4×10^{-6} M) of either the MA or YHMA mutant with varying concentrations of different reactants (i.e., H$_2$O$_2$, sodium azide, CO) at 25 °C and following the spectral evolution in the 380–450 nm wavelength range.

Kinetic progress curves at selected wavelengths were analyzed according to the following equation:

$$OD_{obs} = OD_0 \pm \sum_{i=1}^{i=n} DOD_i \cdot \exp\left(-^i k \cdot t\right) \tag{1}$$

where OD_{obs} is the observed optical density at a selected wavelength and at a given time interval, OD_0 is the optical density at $t = 0$, n is the number of exponentials, DOD_i is the optical density change associated with the exponential i, $^i k$ is the rate constant of the exponential, and t is the time.

The CO dissociation rate constant has been measured by mixing the CO-bound form with a solution of 5 mM sodium nitrite in the presence of 10 mg/mL of sodium dithionite. The data have been analyzed according to Eq. (1).

The pH-dependence of the CO binding kinetics of the ferrous MA and YHMA mutants was carried out by 1:1 mixing in the stopped-flow apparatus of the reduced protein solution (in 1 mM phosphate buffer pH 7.0) with the ligand solution (in 0.15 M phosphate and/or 0.15 M acetate buffer at the desired pH values) and following the spectral evolution in the 380–450 nm wavelength range.

3. Results

3.1. Ferric [Fe(III)] forms

3.1.1. CD spectra

Fig. 1A compares the far-UV CD spectra of wild type (WT) human cyt c and the mutants. The spectra exhibit two minima at 208 nm and 222 nm, typical of α-helix folded proteins. Both the MA and YHMA mutants show a reduction of the CD signal at 222 nm, suggesting a decrease of the α-helix content that is more evident in the YHMA mutant, possibly due to more extensive structural changes induced by the combination of the YH mutation with that of MA. Fig. 1B reports the CD spectra in the Soret region, which for WT human cyt c, shows the usual positive and negative Cotton effect at 408 nm and 416 nm, respectively. Conversely, the Soret CD spectra of the MA and YHMA mutants show a single positive band in the region 400–410 nm and no negative bands, suggesting a significant conformational change of the heme pocket with respect to WT human cyt c. In particular, a change of the distance and orientation of the F82 side chain positioned on the M80 side of the heme plane [18] is suggested. Similar CD spectra were observed when the axial methionine ligand was replaced by His, Lys or OH$^-$ ion [24,14].
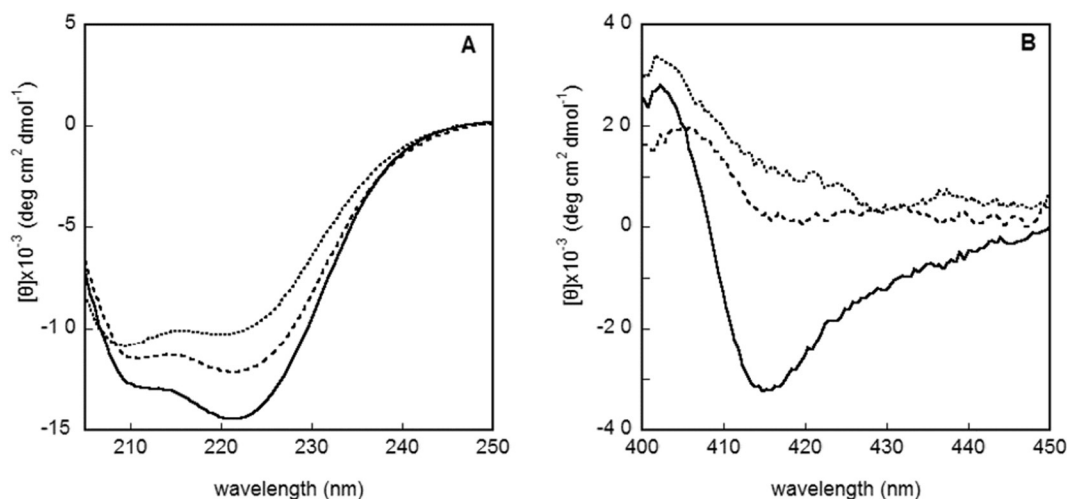

Fig. 1. (Panel A) far-UV CD spectra and (panel B) Soret CD spectra of WT human cyt c (solid line), MA (dashed line) and YHMA (dotted line) in 0.1 M phosphate buffer, pH 7.0, 25 °C, 7 μM protein concentration.

3.1.2. Resonance Raman and UV spectra

3.1.2.1. Met80Ala mutant (MA). The RR and UV–vis spectra of the ferric MA mutant of human cyt *c* are almost identical to those reported for the MA mutant of *S. cerevisiae* cyt *c* [25–27] and horse heart (HH) cyt *c* [22], characterized by the absence of the charge transfer (CT) band at 695 nm (Fig. S1, panel A). At neutral pH the main species is 6 coordinate low spin (6cLS) (Soret maximum at 408 nm) showing RR core size marker bands with slightly upshifted frequencies compared to the WT protein (Fig. S1, panel B). At lower pH, a 6 coordinate high spin (6cHS) aquo form (Soret maximum at 401, CT1 at 625 nm) increases (Fig. 2).

Therefore, the replacement of Met80 with another internal ligand [19,28–32] induces the formation of a more planar heme. The variations in the low frequency region (Fig. 2, *spectrum b*), particularly the down-shift of the ν_8 band (from 349 to 346 cm^{-1}) and the intensity loss of the thioether bending mode [$\delta(C_\beta C_a S)$ at 397 cm^{-1}], suggest that the 6cLS species of the MA mutant of human cyt *c* has a $^-$OH-Fe-His coordination [28], as also observed for the corresponding mutant in iso-cytochrome *c* [27].

The complete vibrational assignment of the RR spectra of the MA mutant in its ferric and ferrous forms is reported in Table S2.

3.1.2.2. Y67H-M80A (YHMA). The double YHMA mutation gives rise to the appearance of two new species, namely (*i*) a misligated 6cLS heme, characterized by a Soret band at 409 nm, and (*ii*) a 6cHS aquo form, with the Soret band at 397 nm and CT1 at 630 nm, which increases at lower pH (Fig. 3, panel A). In the high frequency RR spectra (Fig. S2, *spectrum b*), the core size marker bands of the 6cLS species have frequencies higher than those of the WT (Fig. S2, *spectrum a*); they differ from those of the MA mutant (Fig. S1, *spectrum b*), but are very similar to those of the His-Fe-His complex of horse heart cyt *c*, prepared by addition of SDS/ImH to the WT protein [19] (Fig. S2, *spectrum d*). Moreover, a curve fitting analysis (data not shown) confirms the presence of a 5cHS form.

In the RR low frequency region (Fig. 3, panel B), the observed marked changes compared to WT are consistent with the changes observed when cyt *c* adopts a bis-His coordination (His-Fe-His) [19,24, 32]. In fact, i) the 330–430 cm^{-1} region, called "fingerprint region", due to its sensitivity to the heme ligation, resembles closely the bis-
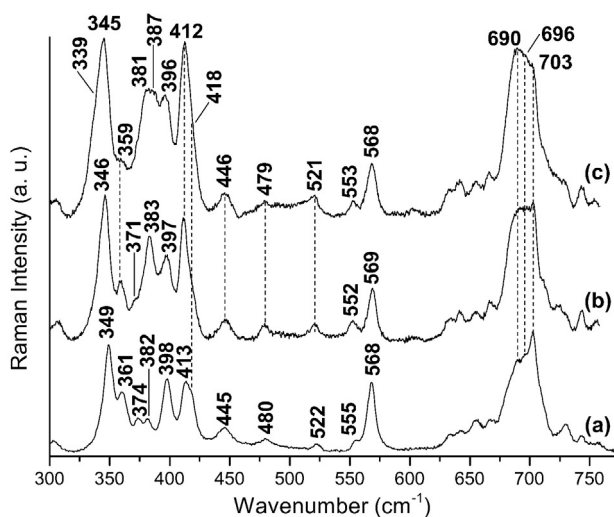

Fig. 2. Comparison of RR spectra in the low frequency region of ferric WT human cyt *c* at pH 7.0 (a) together with its MA mutant at pH 7.0 (b) and pH 5.5 (c). Experimental conditions: 406.7 nm excitation wavelength, laser power at the sample 5 mW (a) and 2 mW (b, c). (a): average of 4 spectra with 20 min integration time; (b): average of 7 spectra with 70 min integration time; (c): average of 12 spectra with 120 min integration time. The intensities are normalized to that of the ν_4 band. The spectra have been shifted along the coordinate axis to allow better visualization.
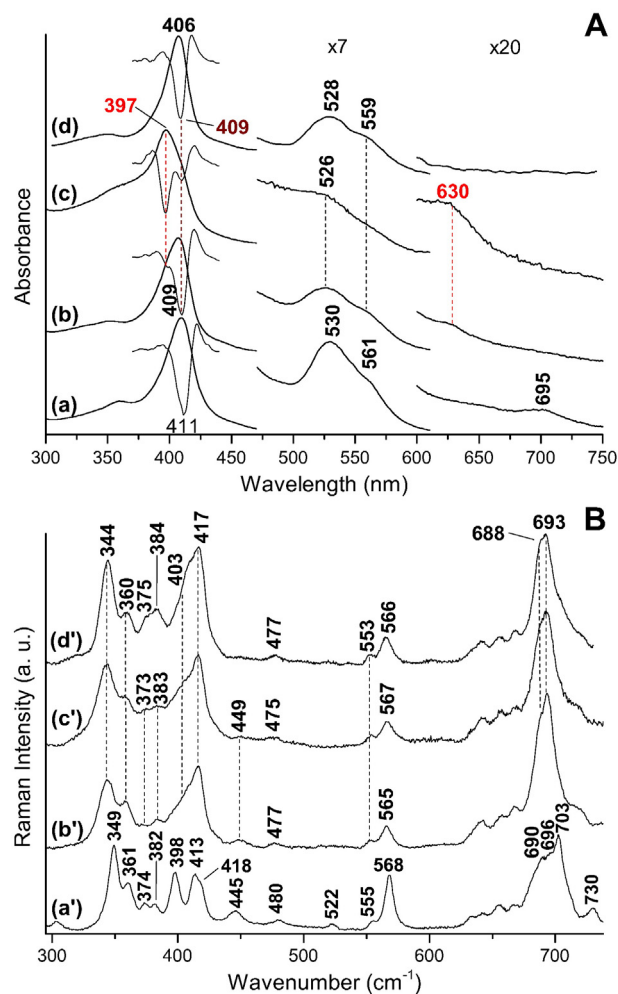

Fig. 3. Comparison of the electronic absorption (Panel A) and RR spectra (Panel B) in the low frequency region of ferric WT human cyt *c* at pH 7.0 (a, a') together with its Y67H/M80A mutant at pH 7.0 (b, b') and pH 5.5 (c, c') and HH cyt *c* after addition of SDS/ImH (d, d'). Panel A: electronic absorption and second derivative spectra, the 470–610 and 600–750 nm regions are expanded 7- and 20-fold, respectively. The spectra have been shifted along the ordinate axis to allow better visualization. Panel B: RR experimental conditions: 406.7 nm excitation wavelength, laser power at the sample 5 mW (a', d') and 2 mW (b', c'). (a'): average of 4 spectra with 20 min integration time; (b'): average of 8 spectra with 40 min integration time; (c'): average of 24 spectra with 120 min integration time; (d'): average of 6 spectra with 30 min integration time. The RR intensities are normalized to that of the ν_4 band. The spectra have been shifted along the ordinate axis to allow better visualization.

His complex of horse heart cyt *c* (Fig. 3, panel B, *spectrum d'*), ii) the decrease in intensity of the out-of-plane bending modes [γ_{22} (445 cm^{-1}), γ_{12} (522 cm^{-1}), γ_{21} (568 cm^{-1}) and γ_5 (730 cm^{-1})] and of the propionyl bending mode [$\delta(C_\beta C_c C_d)$, at 374 cm^{-1}]; iii) the downshift of the ν_8 band to 344 cm^{-1} with the concomitant broadening and intensity decrease; iv) the presence of the very intense band at 417 cm^{-1} [$\delta(C_\beta C_a C_b)$]; v) the shift of the ν_7 band, which overlaps with the ν(C—S) stretching mode at 696 cm^{-1}, are all consistent with such an assignment. Accordingly, the curve fitting analysis of the pH 7.0 double mutant spectrum (Fig. S3) shows the presence of a new band at 403 cm^{-1}, assigned to the bis-His asymmetric stretching mode [ν_{as}(Fe—Im$_2$)], as previously observed in the spectra of the bis-His coordinated N-fragment of cyt *c* and cyt *c''* [24]. Since coordination of His26 or His33 would require a change in the tertiary structure, it is very likely that His67, which replaces Tyr67 in the distal cavity, binds the iron atom. It is noted that the spectra of the M80A, M80A/Y67A, and M80A/Y67H mutants of yeast iso-1 cyt *c* at pH 7.2 revealed the presence of only a $^-$OH-Fe-His18 species [26]. However, the low frequency spectrum of the human YHMA mutant (Fig. 3, panel B) shows no similarities
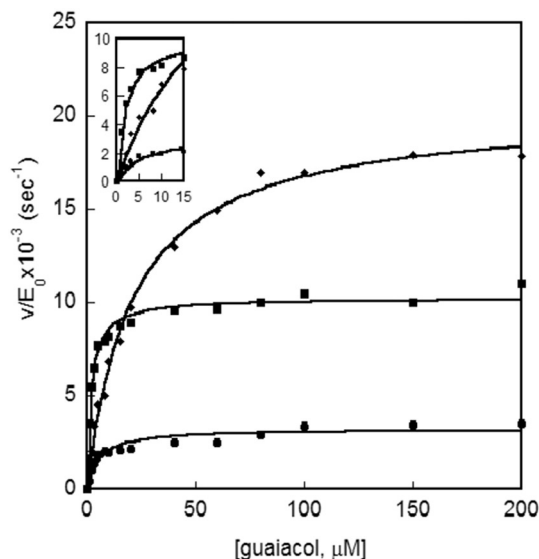
Fig. 4. Steady-state rate *v* of human cyt *c*-catalyzed oxidation as a function of guaiacol concentration. WT (●), MA (■), YHMA (◆). Reaction conditions: 1 μM cyt *c*, 1 mM H_2O_2, at pH 7.0 and 25 °C in 0.1 M phosphate. Continuous lines correspond to the linear least-squares fitting of data according to Eq. (2), employing the parameters reported in Table 1. The inset shows a magnification of the rising part of the hyperbolic curves.

with that reported for the $^-$OH bound yeast YHMA mutant nor with that of human cyt *c* at alkaline pH [14]. Moreover, recently we have found that the single mutation Y67H in human cyt *c* does not alter the protein, which remains very similar to the WT [14].

The complete vibrational assignment of the RR spectra of the YHMA mutant in its ferric and ferrous forms is reported in Table S3.

3.1.3. Peroxidase activity

Analysis of the catalytic activity of WT cyt *c* and mutants has been performed using a typical peroxidase assay that involves guaiacol oxidation by H_2O_2 [23] (Fig. 4). The experiments here reported were performed using 1 mM H_2O_2, an optimum concentration for obtaining product formation without affecting protein and heme integrity. Higher H_2O_2 concentrations may produce oxidative damage [33].

The data were fitted using a non-linear regression analysis according to the Michaelis-Menten equation

$$\frac{v}{[E_0]} = \frac{k_{cat} \cdot [S]}{K_m + [S]} \tag{2}$$

where $[E_0]$ is the human cyt *c* concentration, v is the observed velocity of guaiacol oxidation, $[S]$ is the guaiacol concentration, K_m is the apparent Michaelis-Menten equilibrium constant (corresponding to the affinity of substrate for the enzyme) and k_{cat} is the apparent speed of the rate-limiting step.

At pH 7.0 and 25 °C, WT human cyt *c* exhibits a very low peroxidase activity, with an apparent performance constant (k_{cat}/K_m) comparable

to that of WT horse heart cyt *c* [13]. The MA variant, where cleavage of the Fe-Met80 bond occurs, displays more favorable apparent k_{cat}/K_m values than WT for peroxidation of guaiacol (see Table 1). MA is about 10-fold more efficient, an effect mainly attributable to an approximately 3-fold increased value of k_{cat} and 3-fold decreased value of apparent K_m (see Table 1). Interestingly, k_{cat}/K_m for the peroxidation of guaiacol observed for the cardiolipin/cyt *c* complex (*i.e.*, 3.2×10^3 M^{-1} s^{-1}) [13], in which the heme Met80 axial ligand bond is ruptured, is lower than that reported here for the MA variant. On the other hand, the apparent k_{cat}/K_m value for the human YHMA mutant is only marginally increased with respect to that of the human WT and Y67H mutant [14]. This probably reflects an increase of the hexa-coordinated form due to binding of His67, as suggested by a 4-fold increased value of apparent K_m (see Table 1).

3.1.4. Sodium azide kinetics

Both the MA and YHMA mutants are able to bind sodium azide and display a biphasic kinetic pattern, suggesting the presence of two Fe(III) species, which are interconverting at a much slower rate with respect to the binding reaction described by Scheme 1 (see Fig. 5).

It appears immediately evident that both phases are characterized by a rate-limiting step, according to the classic Scheme 1 [34,35]

$$\textbf{P-L} \underset{k_{+L}}{\overset{k_{-L}}{\rightleftarrows}} \textbf{P+L+N}_3^- \underset{h_{off}}{\overset{h_{on}}{\rightleftarrows}} \textbf{P-N}_3 \tag{Scheme 1}$$

P-L represents a form where the sixth axial coordination of the heme is occupied by a ligand L (which can be either a weakly coordinated H_2O molecule or an endogenous ligand, such as an amino acidic side chain, with dissociation and association rates of k_{-L} and k_{+L}, respectively); h_{on} and h_{off} are the association and dissociation of the exogenous ligand sodium azide N_3^-. Since the intermediate P species is never detected during the observed reaction, for each of the two phases, the observed rate constant h_{obs} (derived from the application of Eq. 1) can be then described by the following equation [34,35]:

$$h_{obs} = \frac{k_{-L} \cdot h_{on} \cdot [N_3^-]}{k_{+L} + h_{on} \cdot [N_3^-]} + \frac{h_{off} \cdot k_{+L}}{k_{+L} + h_{on} \cdot [N_3^-]} \tag{3}$$

and at very high $[N_3^-]$, $h_{obs} \approx k_{-L}$. In this mechanism we can calculate accurately both k_{-L} and h_{off}, whereas we can only obtain the ratio,
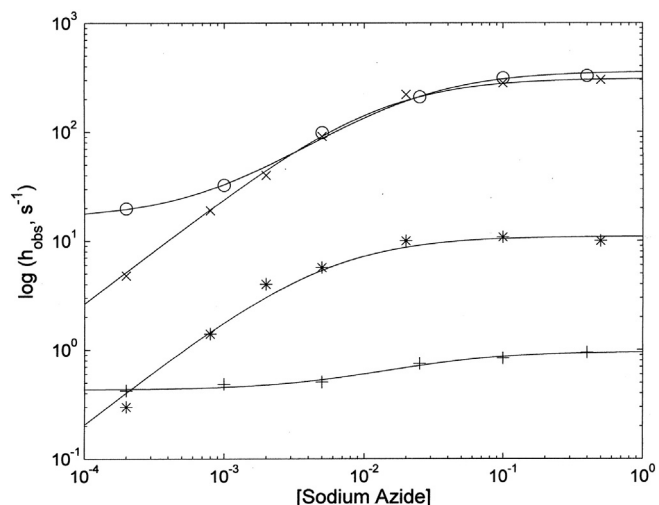

Fig. 5. Dependence of h_{obs} on sodium azide concentration for the MA (o, fast phase; +, slow phase) and the YHMA mutants (x, fast phase; *, slow phase) in 0.1 M phosphate pH 7.0 and 25 °C. Continuous lines have been obtained by non-linear least-squares fitting of the data according to Eq. (3), employing the parameters reported in Table 2.

Table 1
Apparent catalytic parameters for guaiacol oxidation. Reaction conditions for the guaiacol peroxidase activity of WT cyt *c*, MA, YHMA, Tyr67Arg human cytochrome *c* mutant (YR) [14], and YH [14] mutants: 1 μM cyt *c*, 1 mM H_2O_2, at pH 7.0 and 25 °C in 0.1 M phosphate.

Protein	K_m (M) $\times 10^{-6}$	k_{cat} (s^{-1}) $\times 10^{-3}$	k_{cat}/K_m (M^{-1} s^{-1}) $\times 10^2$
WT	3.9 ($\pm$0.4)	3.1 ($\pm$0.4)	7.9 ($\pm$1.8)
MA	1.4 ($\pm$0.2)	10.6 ($\pm$2.0)	78.0 ($\pm$26)
YHMA	15.1 ($\pm$1.5)	19.1 ($\pm$2.1)	12.6 ($\pm$2.2)
YH[a]	8.5 ($\pm$1.7)	7.8 ($\pm$0.9)	9.2 ($\pm$2.1)
YR[a]	5.1 ($\pm$0.8)	32.0 ($\pm$12)	63.0 ($\pm$10)

[a] [14].

Table 2
Parameters for azide binding to the MA and YHMA mutants according to Scheme 1 from Eq. (3).

	MA	YHMA
$^1k_{-L}$ (s^{-1})	360 ($\pm$48)	310 ($\pm$39)
$^1h_{off}$ (s^{-1})	16.1 ($\pm$2.3)	0.42 ($\pm$0.09)
$^1\tau$ ($=^1h_{on}/^1k_{+L}$)	5.2 ($\pm$0.7) $\times$ 10^1	8.3 ($\pm$1.1) $\times$ 10^1
$^2k_{-L}$ (s^{-1})	0.96 ($\pm$0.18)	10.9 ($\pm$1.8)
$^2h_{off}$ (s^{-1})	0.43 ($\pm$0.08)	2.5 ($\pm$0.4) $\times$ 10^{-2}
$^2\tau$ ($=^2h_{on}/^2k_{+L}$)	4.7 ($\pm$0.7) $\times$ 10^1	1.9 ($\pm$0.3) $\times$ 10^2

h_{on}/k_{+L}, of h_{on} and k_{+L}, which we define as the τ parameter. The parameters for the two Fe(III) species are reported in Table 2.

The analysis of the parameters reported in Table 2 indicates that the rate-limiting step for the fast phase is closely similar for both mutants, likely referable to the dissociation of the weakly coordinated H$_2$O of the 6cHS species. Interestingly, the observed rate (see Table 2) is closely similar to that reported for other mutants of yeast iso-cytochrome c upon reaction with sodium azide [36]. On the other hand, the rate limiting step for the slower phase, likely referable to the 6cLS species, is drastically different, clearly suggesting that the more tightly bound endogenous coordinating ligand is different in the two mutants. This proposal is in line with the spectroscopic observation that the sixth axial ligand in the MA mutant is OH$^-$, while it is a His in the YHMA mutant, which clearly suggests that the energy of the Fe-His bond is much lower than that of the Fe-OH$^-$ bond. An additional interesting feature is represented by the sodium azide dissociation rate constants h_{off}, which are clearly much faster for the MA mutant with respect to the YHMA mutant, suggesting a role of the substituting histidine in slowing down ligand dissociation.

3.2. Ferrous [Fe(II)] forms

3.2.1. Spectroscopic measurements

3.2.1.1. Met80Ala (MA). Upon reduction, the UV–Vis spectrum of the MA mutant (Fig. 6, panel A) is characteristic of a mixture of two species, a 6cLS heme (bands at 412, 521, and 550 nm) and a 5cHS form (434 and 565 nm), indicating that the sixth coordination position of the heme iron is partially occupied by an internal ligand. Accordingly, the presence of a small amount of 6cLS species is observed in the high frequency RR spectrum, obtained in resonance with the LS form (413.1 nm) (Fig. 6, panel C, *spectrum* b"). Conversely, the 5cHS species, becomes predominant with excitation at 441.6 nm, *i.e.* in resonance with the Soret band of the 5cHS heme at 434 nm, (Fig. 6, panel C, *spectrum* c"). This effect is markedly evident in the low frequency region as the spectra obtained with the two excitation wavelengths are very different (Fig. 6, panel B, *spectrum* b' and *spectrum* c'). In the 441.6 nm spectrum the strongest band at 236 cm^{-1}, which becomes very weak for 413.1 nm excitation, is tentatively assign to the ν(Fe—Im) stretching mode, since it is expected to give rise to a strong band in 5cHS ferrous heme proteins upon excitation in the Soret band [37]. The nature of the internal ligand responsible for the minor 6cLS species is unclear.

3.2.1.2. Tyr67HisMet80Ala (YHMA). Upon reduction, the electronic absorption spectrum of the YHMA mutant is very similar to that of the WT (Fig. S4, left panel). However, the 6cLS RR spectrum in the high frequency region (Fig. S4, right panel) is characterized by core size marker bands that are up-shifted by 2–4 cm^{-1}. In addition, the bands at 1585 (ν_{19}) and 1547 (ν_{11}) cm^{-1}, which are anomalously intense in the WT spectrum due to distortion of the heme [38], almost disappear in the mutant spectrum. Therefore, as for the ferric state, these changes suggest the formation of a misligated 6cLS ferrous form [39]. Accordingly, the low frequency region spectrum (Fig. 7, *spectrum* YHMA) shows pronounced changes in the relative intensities and frequencies of the bands compared to WT (see the detailed analysis reported in the SI), which
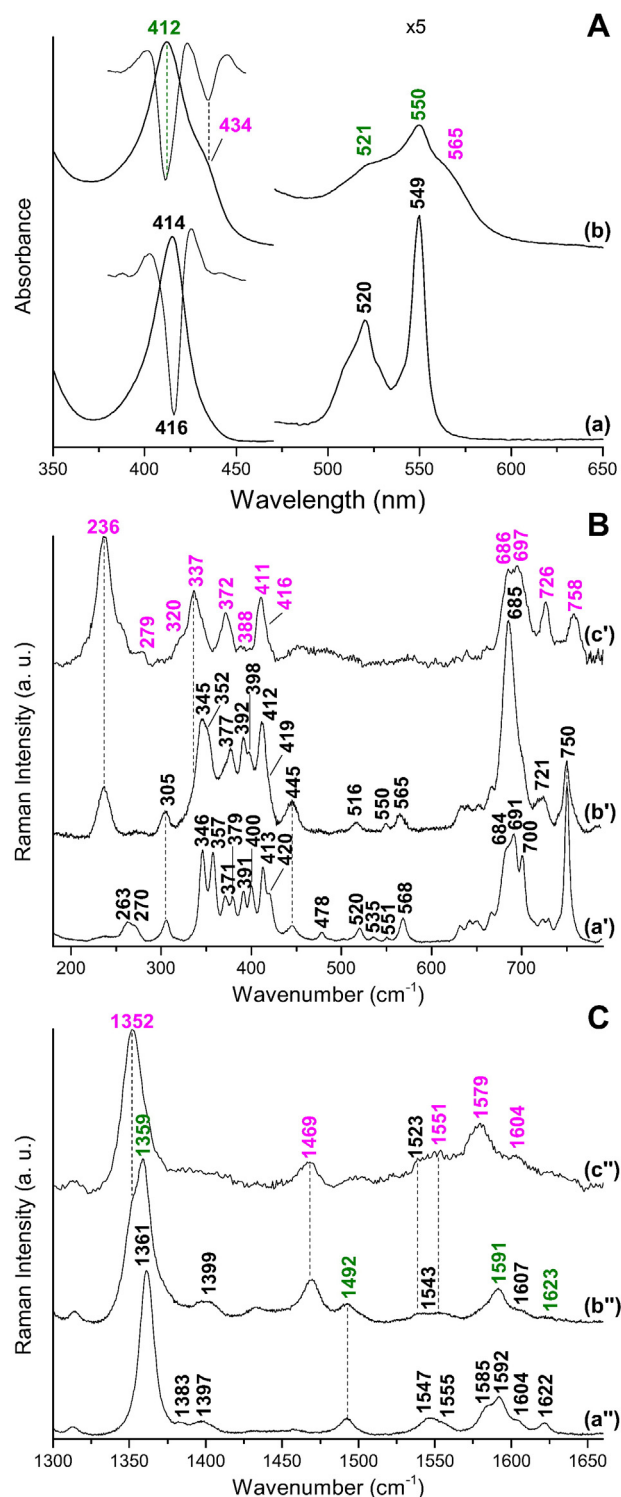

Fig. 6. Electronic absorption (Panel A) and RR spectra in the low (Panel B) and in the high (Panel C) frequency range of ferrous WT human cyt c at pH 7.0 (a, a', a") and of its MA mutant at pH 5.9 (b, b', b", c' and c"). Panel A: the 470–650 region has been expanded 5-fold. Panels B and C: RR spectra experimental conditions: 413.1 nm excitation wavelength. (a', a") laser power at the sample 5 mW, average of 4 spectra with 20 min integration time. (b', b"), laser power at the sample 2 mW, (b'), average of 12 spectra with 60 min integration time. (b") average of 6 spectra with 30 min integration time. 441.6 nm excitation wavelength: (c', c"), laser power at the sample 10 mW, (c'), average of 4 spectra with 20 min integration time. (c") average of 3 spectra with 15 min integration time. The intensities are normalized to that of the ν_4 band. The spectra have been shifted along the ordinate axis to allow better visualization.
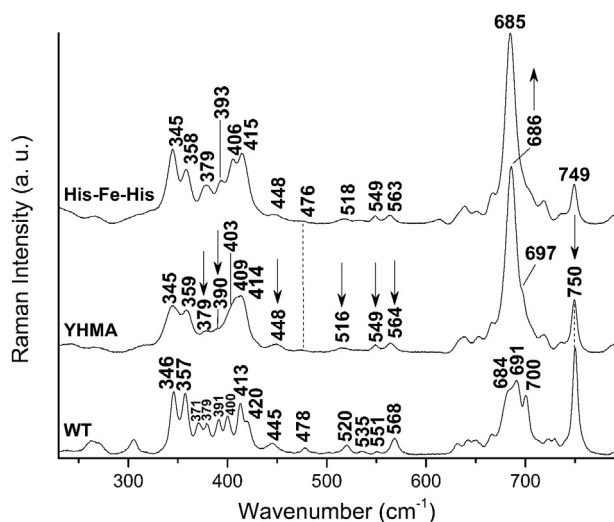
Fig. 7. Comparison of the RR spectra in the low frequency region of ferrous WT and YHMA at pH 7.0 together with WT in SDS/ImH (His-Fe-His). Experimental conditions: 413.1 nm excitation wavelength; (WT, His-Fe-His): laser power at the sample 5 mW, average of 4 spectra with 20 min integration time; (YHMA): laser power at the sample 2 mW, average of 8 spectra with 40 min integration time. The intensities are normalized to that of the ν_4 band. The spectra have been shifted along the ordinate axis to allow better visualization.

indicate that, as for the ferric form, His67 replaces the Met80 ligand in the ferrous form, giving rise to a His-Fe-His18 6cLS species. In fact, the spectrum is very similar to that of the HH cyt c in SDS/ImH His-Fe-His model compound (Fig. 7, *spectrum* His-Fe-His).

3.2.2. Ferrous-CO

Unlike the WT protein, the MA and YHMA mutants bind CO. The sixth ligand of the ferrous form is displaced and a 6cLS CO complex is obtained, characterized by a Soret band at 413 (MA) and 412 nm (YHMA), and Q bands at 530, 564 nm (MA) and 531, 558 nm (YHMA) (Fig. 8, top panel).

Based on ^{13}CO isotopic substitution (Fig. S5), a single conformer has been identified for the MA-CO complex characterized by $[\nu(FeC)]$ at 490 cm^{-1} and $[\nu(CO)]$ at 1961 cm^{-1}. Interestingly, the YHMA-CO complex shows the presence of two conformers, which change relative intensity during irradiation. The main species, which forms immediately upon CO complexation, is characterized by $[\nu(FeC)]$ at 496 cm^{-1} and $[\nu(CO)]$ at 1954 cm^{-1}. After about 30 min, this species decreases in intensity and, concomitantly, a second form ($[\nu(FeC)]$ at 503 cm^{-1} and $[\nu(CO)]$ at 1967 cm^{-1}) becomes predominant.

CO is an excellent probe for investigating the distal cavity of heme proteins [40] because back-donation from the Fe dπ to the CO π* orbitals is modulated by polar interactions and, in particular, by the formation of H-bonds between the bound CO and the distal protein residues. A positively charged electrostatic field favors back-donation, which strengthens the Fe—C bond and correspondingly weakens the CO bond, thereby increasing the $\nu(Fe—C)$ vibrational frequencies and decreasing the $\nu(CO)$ frequencies [41]. A negative linear correlation between the frequencies of the $\nu(Fe—C)$ and $\nu(CO)$ stretching modes has been established for a large class of CO complexes of heme proteins and heme model compounds containing imidazole as the fifth iron ligand [42] (solid line in Fig. 9). The $\nu(Fe—C)/\nu(CO)$ position along the correlation line reflects the type and strength of distal polar interactions [40]. In Fig. 9 and Table 3 the CO adducts of a series of myoglobin (Mb) complexes together with the CO complexes of the human cyt c mutants are reported.
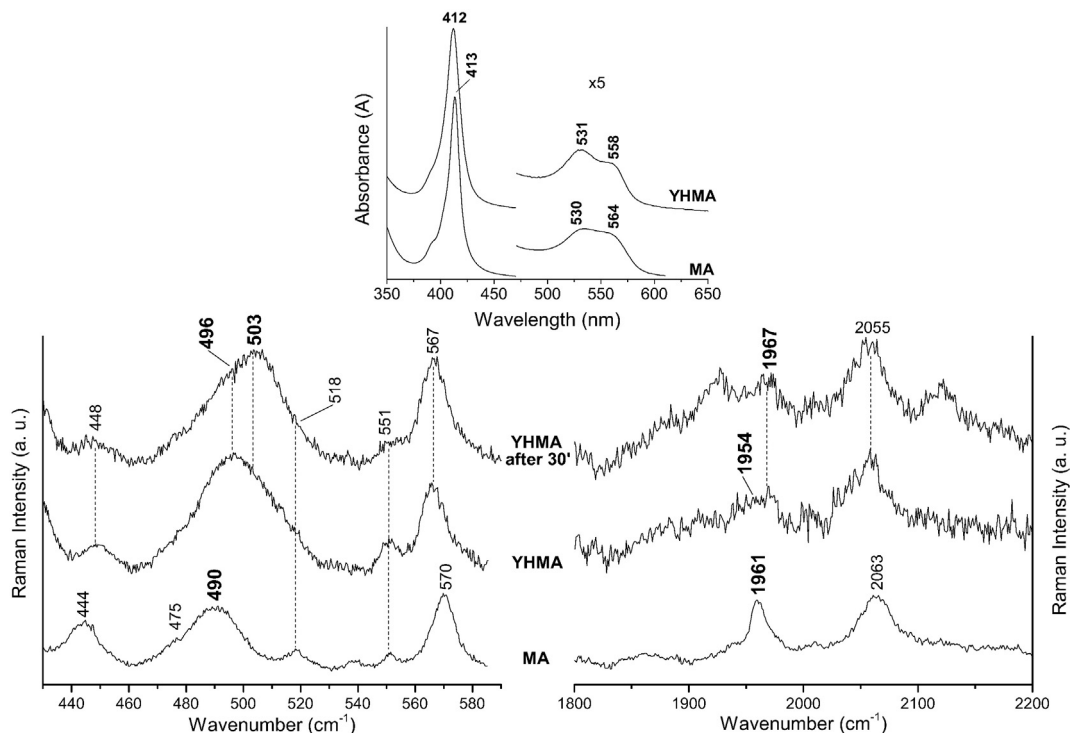

Fig. 8. Fe^{2+}–CO complexes of MA and YHMA at pH 7.0. Top panel: electronic absorption spectra. The 470–650 region has been expanded 5-fold. The spectra have been shifted along the ordinate axis to allow better visualization. Bottom panel: RR spectra obtained with an excitation wavelength of 413.1 nm in the 420–600 cm^{-1} (left) and 1800–2300 (right) cm^{-1} regions, immediately after preparation and after 30 min of irradiation. Experimental conditions: (MA): 2 mW laser power at the sample; (left) average of 4 spectra with 20 min integration time; (right) average of 12 spectra with 120 min integration time; (YHMA, left) 2 mW laser power at the sample; average of 2 spectra with 10 min integration time; (YHMA, right) 1.5 mW laser power at the sample; average of 4 spectra with 40 min integration time; (YHMA, after 30′) 2 mW laser power at the sample; (left) average of 4 spectra with 20 min integration time; (right) average of 4 spectra with 40 min integration time. The spectra in the 1800–2300 cm^{-1} region have been obtained using a 1800 grooves/mm grating.
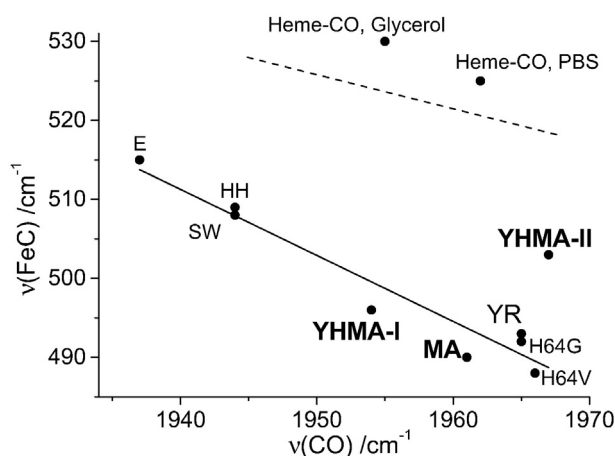
Fig. 9. Correlation plot between the ν(Fe—C) and ν(CO) stretching frequencies of the CO complexes of the cyt c mutants compared with those of different Mbs and selected distal His mutants containing histidine as the proximal ligand (E = elephant, SW = sperm whale, HH = horse heart). The heme-CO adduct in glycerol or in phosphate-buffered saline (PBS) represent examples of five coordinate CO-heme complexes with no trans ligand, in which the correlation line (dashed line) is displaced above that of the proximal histidine-containing proteins (solid line). The frequencies are reported in Table 3.

At neutral pH, the distal histidine residue (H64) of wild-type horse heart (HH) or sperm whale (SW) Mb forms a weak H-bond interaction with the bound CO, resulting in a point located in the central region of the back-bonding line. When the distal histidine is replaced by hydrophobic residues (*e.g.* sperm whale H64V or human H64G mutants) the ν(Fe—C)/ν(CO) point slides down the line reflecting the expected decreased back-bonding. In the absence of a polar interaction between the oxygen atom of CO and a distal residue, the CO is linear and perpendicular to the heme plane. On the contrary, elephant Mb (E) has a glutamine in place of H64 [43], which evidently forms a somewhat stronger H-bond, moving the point above the line relative to the distal histidine-containing species. Variations in the donor strength of the trans-ligand also affect the frequencies. In fact, CO complexes with a weak or absent proximal ligand are located above the histidine line [40]. Hence, the upper dashed line in Fig. 9 represents five-coordinate, with no trans ligand, or six-coordinate heme-CO complexes with weak trans ligands [40]. The cases of the (Fe^{2+}) heme-CO adduct in glycerol [38] or in phosphate-buffered saline (PBS) [39], are shown as examples of CO-heme complexes with no trans ligand.

Similar to the human cyt c Y67R mutant [14], the ν(FeC) and ν(CO) frequencies of the MA-CO complex are located close to those of the Mb H64V and H64G variants, indicating the presence of very weak or absent distal polar interactions between the CO and the distal residues. The first species formed by the double YHMA mutant upon CO addition [with ν(FeC) and ν(CO) at 496 and 1954 cm^{-1}, respectively], shows weak distal polar interactions probably with the His67. The second conformer

Table 3
RR Fe-CO and ν(C—O) stretching frequencies (cm^{-1}) of the MA and YHMA mutants and various myoglobins reported in Fig. 9.

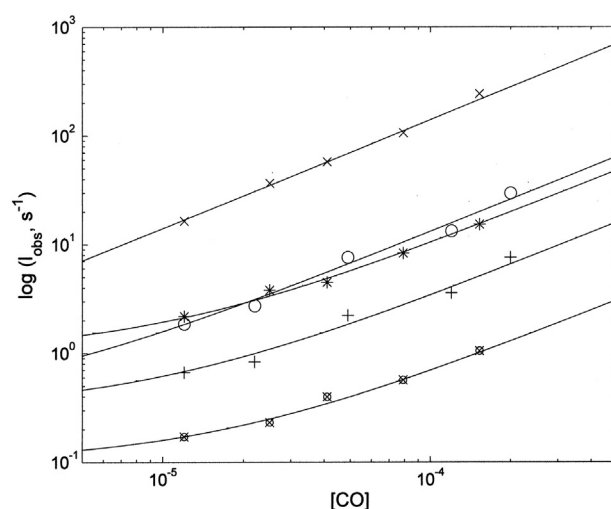| Protein	ν(FeC) (cm^{-1})	ν(CO) (cm^{-1})	Ref.
Elephant Mb	515	1937	[43]
Horse heart Mb, pH 7	509	1944	[44]
Sperm whale Mb pH 7	508	1944	[45]
YHMA-I	**503**	**1967**	**This work**
YHMA-II	**496**	**1954**	**This work**
MA	**490**	**1961**	**This work**
YR human cyt c	493	1965	[14]
H64G Mb (human)	492	1965	[46]
H64V Mb (sperm whale)	488	1967	[47,48]
Heme-CO, glycerol	530	1955	[49]
Heme-CO, PBS	525	1962	[50]

Fig. 10. CO dependence of l_{obs} at pH 7.0 in 0.1 M phosphate buffer at 25 °C for MA (o, fast phase, +, slow phase) and YHMA mutants (x, fast phase, *, intermediate phase, ⊗, slow phase). Continuous lines have been obtained by non-linear least-squares fitting of the data according to Eq. (4), employing the parameters reported in Table 4.

(with ν(FeC) and ν(CO) at 503 and 1967 cm^{-1}, respectively) which increases with time, is located at a somewhat displaced position above the histidine line indicating a weakening of the Fe-Im ligation [50].

3.2.3. CO binding kinetics

Both the MA and YHMA mutants are able to bind CO following a bimolecular CO-dependent behavior (Fig. 10), which can be described according to the following equation:

$$l_{obs} = l_{on} \cdot [CO] + l_{off} \qquad (4)$$

where l_{obs} is the observed rate constant at a given concentration of CO, l_{on} is the CO association rate constant, and l_{off} is the CO dissociation rate constant; the data are reported in Table 4.

In the case of the MA mutant, we observe a biphasic CO binding pattern indicating the presence of two Fe(II) species, which are characterized by different CO association rate constants l_{on}, but with the same ligand dissociation rate l_{off} (Table 4). On the other hand, in the case of the YHMA mutant we observe a CO binding process characterized by three phases, suggesting the occurrence of three forms with different ligand association rate constants. However, only a biphasic CO dissociation process is observed, suggesting that two of the three forms show the same ligand dissociation rate constant l_{off} (Table 4). Nevertheless, for both mutants no rate-limiting step for CO binding was observed for the two (in the case of the M80A mutant) or the three phases (in the case of the double mutant), as instead was observed in the case of the M80A mutant of yeast iso-cytochrome c [51].

The pH-dependence of the CO binding rate constants is reported in Fig. 11, which has been analyzed according to the following equation

Table 4
Kinetic parameters for CO binding at pH 7.0 in 0.1 M phosphate buffer at T = 25 °C.

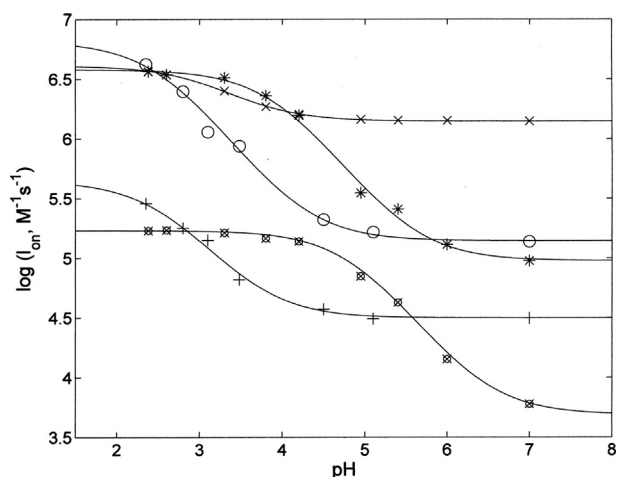|	MA	YHMA
$^{1}l_{on}$ (M^{-1} s^{-1})	1.3 ($\pm$0.3) $\times$ 10^5	1.4 ($\pm$0.3) $\times$ 10^6
$^{1}l_{off}$ (s^{-1})	0.31 ($\pm$0.05)	0.95 ($\pm$0.24)
$^{2}l_{on}$ (M^{-1} s^{-1})	3.2 ($\pm$0.5) $\times$ 10^4	9.5 ($\pm$2.6) $\times$ 10^4
$^{2}l_{off}$ (s^{-1})	0.31 ($\pm$0.05)	0.95 ($\pm$0.21)
$^{3}l_{on}$ (M^{-1} s^{-1})	–	5.9 ($\pm$0.8) $\times$ 10^3
$^{3}l_{off}$ (s^{-1})	–	0.11 ($\pm$0.03)

Fig. 11. pH dependence of the second order rate constant for CO binding to MA (o, fast phase, +, slow phase) and YHMA mutants (x, fast phase, *, intermediate phase, ⊗, slow phase) at 25 °C. Continuous curves have been obtained by non-linear least-squares fitting of the data according to Eq. (5), employing the parameters reported in Table 5.

[52–54]:

$$l_{on} = l_0 \cdot \frac{1}{1 + K_a \cdot [H^+]} + l_H \cdot \frac{K_a \cdot [H^+]}{1 + K_a \cdot [H^+]} \qquad (5)$$

where l_{on} is the observed bimolecular rate constant at a given pH, l_0 is the CO binding bimolecular rate constant of the deprotonated form (at very alkaline pH values) and l_H is the CO binding rate constant of the protonated form, K_a is the proton binding affinity constant ($K_a = 10^{pKa}$) and $[H^+]$ is the proton concentration.

For all the CO binding processes a second-order rate constant enhancement is observed upon decreasing the pH (see Fig. 11), even though this feature displays different characteristics for the various phases and for the two investigated mutants.

The pH dependence of CO binding to the MA and YHMA mutants (Fig. 11, Table 5) clearly indicates that (i) the pK_a of the pH-dependent transition are similar for the two populations of the MA mutant but are lower than those displayed by the double mutant YHMA, likely due to the protonation of the proximal His18, (ii) pK_a values observed for the three populations of the double mutant are progressively higher for the slower reacting species possibly suggesting that, unlike the pH-dependent transition of the fast-reacting population (i.e., pK_{a1} of the YHMA mutant, which is likely attributable to the protonation of the proximal His18), pK_{a2} and pK_{a3} of the double mutant correspond to the protonation of other residues which have an influence on the CO binding process, (iii) the second-order rate constants of the protonated forms (i.e., l_H, see Eq. (4)) are closely similar for the two faster phases of the mutants, with the intermediate population of the YHMA mutant being only slightly slower (see ^2l_H of the YHMA in Table 5), while the

Table 5
Parameters characterizing the proton-linked behavior of CO binding to the MA and YHMA mutants according to Eq. (5).

	MA	YHMA
$^1l_0$ (M^{-1} s^{-1})	1.4 ($\pm$0.3) × 10^5	1.4 ($\pm$0.4) × 10^6
^1l_H (M^{-1} s^{-1})	6.5 ($\pm$1.0) × 10^6	4.1 ($\pm$0.8) × 10^6
pK_{a1}	2.55 ($\pm$0.17)	3.13 ($\pm$0.18)
$^2l_0$ (M^{-1} s^{-1})	3.2 ($\pm$0.5) × 10^4	9.5 ($\pm$2.1) × 10^4
^2l_H (M^{-1} s^{-1})	4.4 ($\pm$0.7) × 10^5	3.8 ($\pm$0.6) × 10^6
pK_{a2}	2.55 ($\pm$0.17)	3.93 ($\pm$0.16)
$^3l_0$ (M^{-1} s^{-1})	–	4.9 ($\pm$0.7) × 10^3
^3l_H (M^{-1} s^{-1})	–	1.7 ($\pm$0.4) × 10^5
pK_{a3}	–	4.87 ($\pm$0.17)

slowest populations of both mutants have a 10–20 fold slower CO binding rate constant (see ^2l_H of MA and ^3l_H of YHMA in Table 5).

4. Discussion

Cyt c is characterized by the presence of an active site heme c prosthetic group covalently bound to the protein moiety, which is axially coordinated in the native form by two residues, namely His18 and Met80. On the distal side of the heme pocket (where Met80 is positioned), there are additional residues (i.e., forming the helix between residues 59 and 69), which play a role in shaping the topology of this portion of the distal pocket by connecting two Ω loops (formed by residues between positions 40 and 57 on one side and by residues between positions 71 and 85 on the other side). The overall structural arrangement is maintained by an H-bond network, which also keeps Met80 in position. Recently, we have shown that Tyr67 plays a crucial role in maintaining this structure in human cyt c [14]. However, although the amino acid sequence of human and yeast cyt c share about 70% identity [10], major differences between these two cytochromes are found for the surface amino acid residues involved in cardiolipin binding and modulation of the peroxidase activity [23]. Therefore, caution must be used when comparing conformational stability and peroxidase activity between various cyt c proteins. In this work, we have studied human cyt c investigating (i) the importance of Met80 by Ala substitution, thus disrupting the axial coordination, and (ii) the additional effect of the substitution of Tyr67 by His, producing a double mutant Y67H/M80A. The comparison of the properties of these two mutants should help to clarify the reciprocal effect of these two residues in regulating the access of exogenous molecules into the heme pocket of human cyt c.

In human and yeast cyt c, mutation of Met80 to Ala leads to significant spectral changes with respect to the WT, which are clearly attributable to the loss of the Met80–heme bond. This event then leads to the appearance of peroxidase activity in cyt c, a significant feature in the early stages of apoptosis. In spite of the absence of the Fe-Met80 bond, the human YHMA double mutant shows only a marginal increase of peroxidase activity with respect to WT and the single YH mutant reported previously ([14] and Table 1). The observation that (i) a significant peroxidase activity is present both in the YR and MA mutants, (ii) the substitution of the Tyr67 by His leads to a marked reduction of the peroxidase activity in the YHMA double mutant and to a WT-like behavior in the YH mutant [14], suggests that the peroxidase activity of cyt c is linked to an overall conformational change of the heme pocket and not only to the disappearance of the Fe-Met80 bond [14,11]. In the present study, the apparent k_{cat}/K_m value of the MA variant is about ten-fold greater than that of the WT protein. This behavior is accompanied by the appearance of two heme species characterized by the substitution of Met80 with either OH$^-$ or H$_2$O (Fig. 12). On the other hand, the apparent k_{cat}/K_m value for the human YHMA mutant is drastically decreased, being similar to that reported for WT human cyt c. This behavior can be associated with the observation that in the ferric form of the YHMA double mutant a 6cHS aquo form coexists with a 6cLS species where the Met80 ligand is replaced by a His residue, likely the His67 residue introduced by mutation (Fig. 12).

The existence of two species (i.e., Fe-H$_2$O and Fe-OH$^-$ in the MA mutant and Fe-H$_2$O and Fe-His in the YHMA mutant) is also reflected in the functional behavior of the mutants, which both show a biphasic reaction pattern with an exogenous ligand, such as sodium azide (see Fig. 5). However, it is important to underline that for both mutants the reaction with the exogenous ligand is rate-limited by the dissociation of the hexa-coordinating ligand (see Scheme 1 and Eq. (3)). In fact, the faster-reacting species of both mutants are characterized by a closely similar value for the rate-limiting step (i.e., $k_{-L} = 360 \pm 48$ s^{-1} for the MA mutant and 310 ± 39 s^{-1} for the YHMA mutant, see Scheme 1 and Table 2), suggesting that the exit rate of the coordinating H$_2$O molecule is similar for the two mutants and is not significantly affected by the residue in position 67. Conversely, the rate-limiting step
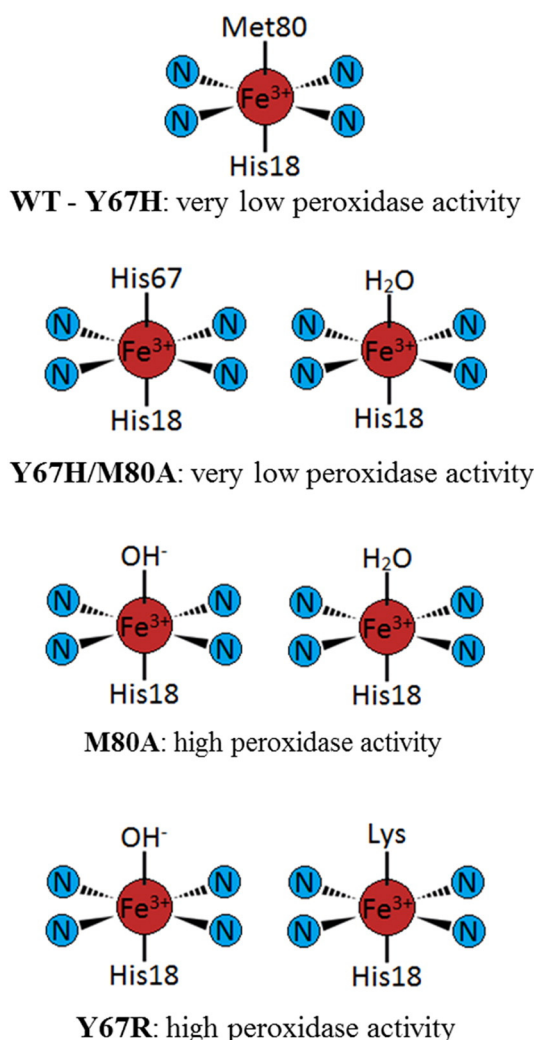
Fig. 12. Schematic representations of the heme coordination following the Met80Ala and Tyr67His/Met80Ala mutations in human cyt *c*. The heme coordination of the previously reported Tyr67His and Tyr67Arg mutants is shown for comparison [14].

for the slow-reacting species is drastically different between the two mutants, being about 10-fold faster in the YHMA mutant (see Fig. 5 and Table 2), indicating that the displacement of the sixth axial ligand by sodium azide is easier in the YHMA double mutant than in the MA variant. This suggests that in the latter case the interaction of His67 with the heme iron is weaker than that of OH⁻ in the MA mutant. The substitution of Tyr67 by His also has a significant effect on the stabilization of the bound azide anion, since its dissociation rate is 20–40 fold slower in the YHMA mutant with respect to the MA species.

In the case of the ferrous form, the spectroscopic evidence that in the MA mutant there is a 5cHS species coexisting with a 6cLS species is reflected in the biphasic CO binding kinetic pattern with two different second-order rate constants (see Fig. 10 and Table 4). In particular, the fast-reacting form is characterized by a rate constant about 4-fold slower (see Table 4) than that observed for mammalian Mbs [52] and about two-fold slower than that reported for the M80A mutant of iso-cytochrome *c* [51], while the slow-reacting form displays a rate constant about five times slower than the faster phase. The evidence that for both the 5cHS and the 6cLS Fe(II) forms of the MA mutant the CO binding rate constant displays a bimolecular behavior clearly indicates that, unlike for iso-cytochrome *c* [51], the hexa-coordinating ligand in the 6cLS form dissociates at a rate faster than the CO binding, suggesting that it is not strongly coordinated to the heme iron. We can rule out the possibility that the structural basis for this functional difference resides in the conformation of the proximal portion of the heme pocket, since the pK_a of the proximal His18 protonation, bringing about the cleavage of the proximal Fe(II)-His18 bond, appears closely similar for the two species (see Fig. 11 and Table 5). Therefore, the experimental evidence that the two species display drastically different CO binding bimolecular rate constants also for the protonated form (*i.e.*, l_H, see Table 5) indeed suggests that their functional differences stem from two different structural arrangements of the distal portion of the heme pocket, while the proximal bond displays a similar strength. Interestingly, both forms also have a very similar CO dissociation rate constant. This suggests that there is only one CO-bound conformer, as also indicated by the RR data of the MA-CO complex (see Fig. 8 and Table 3), and that the differences between the two species before CO binding disappear once the Fe(II)-CO complex is formed.

On the other hand, in the case of the double YHMA mutant we observe two CO-ligated species (see Fig. 8 and Table 3), indicating that in this case even in the Fe(II)-CO form two distinct species coexist. This finds functional support in the observation that the CO dissociation process in the YHMA mutant is biphasic (see Table 4). However, the situation for this double mutant is complicated by the fact that CO binding is characterized by three exponentials, all corresponding to bimolecular processes (see Fig. 10). The fastest-reacting species of the YHMA mutant is three-fold faster than that observed in most Mbs (and 10-fold faster than for the MA mutant), while the intermediate species displays a rate closely similar to the faster species of the MA mutant. These two species apparently show a closely similar CO dissociation rate constant (see Table 4), suggesting that they both correspond to the 5cHS species and their functional differences are likely attributable to heterogeneity in the conformation of the heme pocket. This interpretation is indirectly confirmed by the proton-linked behavior of these two species (see Fig. 11 and Table 5), since upon cleavage of the Fe(II)-His18 proximal bond their rates seem to converge towards a very similar value, even though the pK_a of the transition (and thus the strength of the proximal bond) is drastically different. Therefore, it appears that the two species are characterized by a different proximal conformation of the heme pocket, corresponding to a different second-order CO binding rate constant [52,53]. The slowest-reacting form of the YHMA mutant (likely referable to the 6cLS species), displays a very slow CO binding second-order rate constant, much slower than that of the MA mutant (see Table 5). This suggests that although it displays a bimolecular behavior, its rate is affected by a more tightly bound hexa-coordinating residue, which competes more efficiently with the exogenous CO molecule. Interestingly, it is also characterized by a slower CO dissociation rate constant (see Table 4).

In conclusion, on the basis of both the present and previous work [14], it is evident that in human cyt *c* there is an interplay between the two residues at positions 67 and 80 that affects the conformation of the distal side of the heme pocket, and thus the sixth coordination of the heme. Furthermore, this effect seems linked to the substituting residue, since replacement of Tyr67 by Arg (*i.e.*, in YR) leads to the cleavage of the Fe-Met80 bond, whereas mutation of Tyr67 with His (*i.e.*, in YH) leaves human cyt *c* hexa-coordinated and unreactive with exogenous ligands [14]. Interestingly, the replacement of Tyr67 by His in the absence of the Fe-Met80 bond in the YHMA double mutant induces coordination of a new residue (likely the mutated His67). Hence, together with the observation that Tyr67 and/or His 67 do not perturb the Fe-Met80 bond while Arg67 does, it appears likely that the heme sixth axial coordination is regulated by the size of the residue at position 67. Thus, in the absence of the Fe-Met80 bond, His67 is able to coordinate to the heme iron while Tyr67 is not able to interact with the heme iron, confirming the importance of the type of residue at position 67.

Acknowledgements

Appendix A. Supplementary data

Supplementary data to this article can be found online at http://dx.doi.org/10.1016/j.jinorgbio.2017.01.008.

References

[1] S. Orrenius, V. Gogvadze, B. Zhivotovsky, Mitochondrial oxidative stress: implications for cell death, Annu. Rev. Pharmacol. Toxicol. 47 (2007) 143–183.

[2] P. Caroppi, F. Sinibaldi, L. Fiorucci, R. Santucci, Apoptosis and human diseases: mitochondrion damage and lethal role of cytochrome c as proapoptotic protein, Curr. Med. Chem. 16 (2009) 4058–4065.

[3] Y.-L.P. Ow, D.R. Green, Z. Hao, T.W. Mak, Cytochrome c: functions beyond respiration, Nat. Rev. Mol. Cell Biol. 9 (2008) 532–542.

[4] R. Santucci, F. Sinibaldi, A. Patriarca, D. Santucci, L. Fiorucci, Misfolded proteins and neurodegeneration: role of non-native cytochrome c in cell death, Expert Rev. Proteomics 7 (2010) 507–517.

[5] A. Patriarca, T. Eliseo, F. Sinibaldi, M.C. Piro, R. Melis, et al., ATP acts as a regulatory effector in modulating structural transitions of cytochrome c: implications for apoptotic activity, Biochemistry 48 (2009) 3279–3287.

[6] L.C. Godoy, C. Muñoz-Pinedo, L. Castro, S. Cardaci, C.M. Schonhoff, et al., Disruption of the M80-Fe ligation stimulates the translocation of cytochrome c to the cytoplasm and nucleus in nonapoptotic cells, Proc. Natl. Acad. Sci. U. S. A. 106 (2009) 2653–2658.

[7] V.E. Kagan, V.A. Tyurin, J. Jiang, Y.Y. Tyurina, V.B. Ritov, et al., Cytochrome c acts as a cardiolipin oxygenase required for release of proapoptotic factors, Nat. Chem. Biol. 1 (2005) 223–232.

[8] N.A. Belikova, Y.A. Vladimirov, A.N. Osipov, A.A. Kapralov, V.A. Tyurin, M.V. Potapovich, L.V. Basova, J. Peterson, I.V. Kurnikov, V.E. Kagan, Peroxidase activity and structural transitions of cytochrome c bound to cardiolipin-containing membranes, Biochemistry 45 (2006) 4998–5009.

[9] F. Sinibaldi, G. Mei, F. Polticelli, M.C. Piro, B.D. Howes, et al., ATP specifically drives refolding of non-native conformations of cytochrome c, Protein Sci. 14 (2005) 1049–1058.

[10] S. Bandi, B.E. Bowler, Effect of an Ala81His mutation on the Met80 loop dynamics of iso-1-cytochrome c, Biochemistry 54 (2015) 1729–1742.

[11] T. Ying, Z.-H. Wang, Y.-W. Lin, J. Xie, X. Tan, Z.-X. Huang, Tyrosine-67 in cytochrome c is a possible apoptotic trigger controlled by hydrogen bonds via a conformational transition, Chem. Commun. 30 (2009) 4512–4514.

[12] S. Casalini, G. Battistuzzi, M. Borsari, C.A. Bortolotti, G. Di Rocco, A. Ranieri, M. Sola, Electron transfer properties and hydrogen peroxide electrocatalysis of cytochrome c variants at positions 67 and 80, J. Phys. Chem. B 114 (2010) 1698–1706.

[13] A. Patriarca, F. Polticelli, M.C. Piro, F. Sinibaldi, G. Mei, M. Bari, R. Santucci, L. Fiorucci, Conversion of cytochrome c into a peroxidase: inhibitory mechanisms and implication for neurodegenerative diseases, Arch. Biochem. Biophys. 522 (2012) 62–69.

[14] L. Tognaccini, C. Ciaccio, V. D'oria, M. Cervelli, B.D. Howes, M. Coletta, P. Mariottini, G. Smulevich, L. Fiorucci, Structure-function relationships in human cytochrome c: the role of tyrosine 67, J. Inorg. Biochem. 155 (2016) 56–66.

[15] W. Lan, Z. Wang, Z. Yang, T. Ying, X. Zhang, X. Tan, M. Liu, C. Cao, Z.X. Huang, Structural basis for cytochrome c Y67H mutant to function as a peroxidase, PLoS One 9 (9) (2014), e107305.

[16] M.E. Goldes, M.E. Jeakins-Cooley, L.J. McClelland, T.C. Mou, B.E. Bowler, Disruption of a hydrogen bond network in human versus spider monkey cytochrome c affects heme crevice stability, J. Inorg. Biochem. S0162-0134 (2016) 30156–30162.

[17] G. Silkstone, G. Stanway, P. Brzezinski, M.T. Wilson, Production and characterisation of Met80X mutants of yeast iso-1-cytochrome c: spectral, photochemical and binding studies on the ferrous derivatives, Biophys. Chem. 98 (2002) 65–77.

[18] A. Olteanu, C.N. Patel, M.M. Dedmon, S. Kennedy, M.W. Linhoff, C.M. Minder, P.R. Potts, M. Deshmukh, G.J. Pielak, Stability and apoptotic activity of recombinant human cytochrome c, Biochem. Biophys. Res. Commun. 312 (2003) 733–740.

[19] S. Oellerich, H. Wackerbarth, P. Hildebrandt, Spectroscopic characterization of nonnative conformational states of cytochrome c, J. Phys. Chem. B 106 (2002) 6566–6580.

[20] B.S. Rajagopal, G.G. Silkstone, P. Nicholls, M.T. Wilson, J.A.R. Worrall, An investigation into cardiolipin acyl chain insertion site in cytochrome c, Biochim. Biophys. Acta Bioenerg. 1817 (2012) 780–791.

[21] E. Margoliash, N. Frohwirt, Spectrum of horse heart cytochrome c, Biochem. J. 71 (1959) 570–572.

[22] K.L. Bren, H.B. Gray, Structurally engineered cytochromes with novel ligand-binding sites: oxy and carbon monoxy derivatives of semisynthetic horse heart Ala80 cytochrome c, J. Am. Chem. Soc. 115 (1993) 10382–10383.

[23] L.J. McClelland, T.C. Mou, M.E. Jeakins-Cooley, S.R. Sprang, B.E. Bowler, Structure of a mitochondrial cytochrome c conformer competent for peroxidase activity, Proc. Natl. Acad. Sci. U. S. A. 111 (2014) 6648–6653.

[24] E. Santoni, S. Scatragli, F. Sinibaldi, L. Fiorucci, R. Santucci, G. Smulevich, A model for the misfolded bis-His intermediate of cytochrome c: the 1–56 N-fragment, J. Inorg. Biochem. 98 (2004) 1067–1077.

[25] Y. Lu, D.R. Casimiro, K.L. Bren, J.H. Richards, H.B. Gray, Structurally engineered cytochromes with unusual ligand-binding properties: expression of Saccharomyces cerevisiae Met-80 → Ala iso-l-cytochrome c, Proc. Natl. Acad. Sci. U. S. A. 90 (1993) 11456–11459.

[26] G. Battistuzzi, C.A. Bortolotti, M. Bellei, G. Di Rocco, J. Salewski, P. Hildebrandt, M. Sola, Role of Met80 and Tyr67 in the low-pH conformational equilibria of cytochrome c, Biochemistry 51 (2012) 5967–5978.

[27] G.G. Silkstone, C.E. Cooper, D. Svistunenko, M.T. Wilson, EPR and optical spectroscopic studies of Met80X mutants of yeast ferricytochrome c. Models for intermediates in the alkaline transition, J. Am. Chem. Soc. 127 (2005) 92–99.

[28] S. Döpner, P. Hildebrandt, F.I. Resell, A.G. Mauk, Alkaline conformational transitions of ferricytochrome c studied by resonance Raman spectroscopy, J. Am. Chem. Soc. 120 (1998) 11246–11255.

[29] C. Indiani, G. De Sanctis, F. Neri, H. Santos, G. Smulevich, M. Coletta, Effect of pH on axial ligand coordination of cytochrome c″ from Methylophilus methylotrophus and horse heart cytochrome c, Biochemistry 39 (2000) 8234–8242.

[30] J. Zheng, S. Ye, T. Lu, T.M. Cotton, G. Chumanov, Circular dichroism and resonance raman comparative studies of wild type cytochrome c and F82H mutant, Biopolymers 57 (2000) 77–84.

[31] F. Sinibaldi, M.C. Piro, B.D. Howes, G. Smulevich, F. Ascoli, R. Santucci, Rupture of the H-bond linking two omega-loops induces the molten globule state at neutral pH in cytochrome c, Biochemistry 42 (2003) 7604–7610.

[32] P. Caroppi, F. Sinibaldi, E. Santoni, B.D. Howes, L. Fiorucci, T. Ferri, F. Ascoli, G. Smulevich, R. Santucci, The 40′s omega-loop plays a critical role in the stability and the alkaline conformational transition of cytochrome c, J. Biol. Inorg. Chem. 9 (2004) 997–1006.

[33] J.A. Villegas, A.G. Mauk, R. Vazquez-Duhalt, A cytochrome c variant resistant to heme degradation by hydrogen peroxide, Chem. Biol. 7 (2000) 237–244.

[34] N. Sutin, J.K. Yandell, Mechanism of the reactions of cytochrome c. Rate and equilibrium constants for ligand binding to horse heart ferricytohrome c, J. Biol. Chem. 247 (1972) 6932–6936.

[35] M. Coletta, M. Angeletti, G. De Sanctis, L. Cerroni, B. Giardina, G. Amiconi, P. Ascenzi, Kinetic evidence for the existence of a rate-limiting step in the reaction of ferric hemoproteins with anionic ligands, Eur. J. Biochem. 235 (1996) 49–53.

[36] S.P. Rafferty, M. Smith, A.G. Mauk, Azide binding and active site dynamics of position-82 variants of ferricytochrome c, Inorg. Chim. Acta 242 (1996) 171.

[37] T.G. Spiro, X.-Y. Li, in: T.G. Spiro (Ed.), Biological Applications of Raman Spectroscopy, John Wiley & Sons, Inc., New York 1988, pp. 1–37 (3).

[38] S. Hu, I.K. Morris, J.P. Singh, K.M. Smith, T.G. Spiro, Complete assignment of cytochrome c resonance Raman spectra via enzymic reconstitution with isotopically labeled hemes, J. Am. Chem. Soc. 115 (1993) 12446–12458.

[39] S. Othman, A. Desbois, Resonance Raman investigation of lysine and N-acetylmethionine complexes of ferric and ferrous microperoxidase. Influences of the axial ligation on the heme c structure, Eur. Biophys. J. 28 (1998) 12–25.

[40] T.G. Spiro, I.H. Wasbotten, CO as a vibrational probe of heme protein active sites, J. Inorg. Biochem. 99 (2005) 34–44.

[41] G.N. Phillips Jr., M.L. Teodoro, T. Li, B. Smith, J.S. Olson, Bound CO is a molecular probe of electrostatic potential in the distal pocket of myoglobin, J. Phys. Chem. B 103 (1999) 8817–8829.

[42] E.A. Kerr, N.-T. Yu, Vibrational modes of coordinated CO, CN– and NO, in: T.G. Spiro (Ed.), Biological Applications of Raman Spectroscopy. 3, John Wiley and Sons, Inc., New York 1988, pp. 39–95.

[43] E.A. Kerr, N.T. Yu, D.E. Bartnicki, H. Mizukami, Resonance Raman studies of CO and O_2 binding to elephant myoglobin (distal His(E7)Gln), J. Biol. Chem. 260 (1985) 8360–8365.

[44] G. Smulevich, A.R. Mantini, M. Paoli, M. Coletta, G. Geraci, Resonance Raman studies of the heme active site of the homodimeric myoglobin from Nassa mutabilis: a peculiar case, Biochemistry 34 (1995) 7507–7516.

[45] J. Ramsden, T.G. Spiro, Resonance Raman evidence that distal histidine protonation removes the steric hindrance to upright binding of carbon monoxide by myoglobin, Biochemistry 28 (1989) 3125–3128.

[46] D. Morikis, P.M. Champion, B.A. Springer, S.G. Sligar, Resonance Raman investigations of site-directed mutants of myoglobin: effects of distal histidine replacement, Biochemistry 28 (1989) 4791–4800.

[47] J. Ling, T.S. Li, J.S. Olson, D.F. Bocian, Identification of the iron-carbonyl stretch in distal histidine mutants of carbon monoxy myoglobin, Biochim. Biophys. Acta 1188 (1994) 417–421.

[48] T.S. Li, M.L. Quillin, G.N. Phillips, J.S. Olson, Structural determinants of the stretching frequency of CO bound to myoglobin, Biochemistry 33 (1994) 1433–1446.

[49] X. Ye, A. Yu, G.Y. Georgiev, F. Gruia, D. Ionascu, W. Cao, J.T. Sage, P.M. Champion, CO rebinding to protoheme: investigations of the proximal and distal contributions to the geminate rebinding barrier, J. Am. Chem. Soc. 127 (2005) 5854–5861.

[50] F.P. Nicoletti, B.D. Howes, M. Fittipaldi, G. Fanali, M. Fasano, P. Ascenzi, G. Smulevich, Ibuprofen induces an allosteric conformational transition in the heme complex of human serum albumin with significant effects on heme ligation, J. Am. Chem. Soc. 130 (2008) 11677–11688.

[51] G. Silkstone, A. Jasaitis, M.T. Wilson, M.H. Vos, Ligand dynamics in an electron transfer protein. Picosecond geminate recombination of carbon monoxide to heme in mutant forms of cytochrome c, J. Biol. Chem. 282 (2007) 1638–1649.

[52] M. Coletta, P. Ascenzi, T.G. Traylor, M. Brunori, Kinetics of carbon monoxide binding to monomeric hemoproteins. Role of the proximal histidine, J. Biol. Chem. 260 (1985) 4151–4155.

[53] M. Coletta, P. Ascenzi, M. Brunori, Kinetic evidence for a role of heme geometry on the modulation of carbon monoxide reactivity in human hemoglobin, J. Biol. Chem. 263 (1988) 18286–18289.

[54] Y. Cao, F.P. Nicoletti, G. De Sanctis, A. Bocedi, C. Ciaccio, F. Gullotta, G. Fanali, G.R. Tundo, A. Di Masi, M. Fasano, G. Smulevich, P. Ascenzi, M. Coletta, Evidence for pH-dependent multiple conformers in iron(II) heme-human serum albumin: spectroscopic and kinetic investigation of carbon monoxide binding, J. Biol. Inorg. Chem. 17 (2012) 133–147.